Propagation of Airy-related beams

M. I. Carvalho [1,*] **and M. Facão** [2]

[1] *DEEC/FEUP and INESCPorto, University of Porto, 4200-465 Porto, Portugal*
[2] *Department of Physics, I3N, University of Aveiro, 3810-193 Aveiro, Portugal*
[*] *Corresponding author: mines@fe.up.pt*

Abstract: New types of finite energy Airy beams are proposed. We consider two different types of beams, namely, beams that are obtained as blocked and exponentially attenuated versions of Airy functions Ai and Bi, and beams of finite width but having the Airy functions typical phase. All of them show very interesting properties, such as parabolic trajectories for longer propagation distances, profile evolution exhibiting less diffraction, or better definiteness of the main peak, when compared with other finite energy Airy beams studied before.

OCIS codes: (050.1940) Diffraction; (260.2110) Electromagnetic optics; (350.5500) Propagation.

References and links

1. M. V. Berry and N. L. Balazs, "Nonspreading wave packets," Am. J. Phys. **47**, 264–267 (1979).
2. J. Durin, "Exact solutions for nondiffracting beams. I. The scalar theory," J. Opt. Soc. Am. A **4**, 651–654 (1987).
3. J. Durnin, J. J. Miceli, and J. H. Eberly, "Diffraction-free beams," Phys. Rev. Lett. **58**, 1499–1501 (1987).
4. F. Gori, G. Guattari, and C. Padovani, "Bessel-Gauss beams," Opt. Commun. **64**, 491–495 (1987).
5. M. A. Bandres, "Accelerating parabolic beams," Opt. Lett. **33**, 1678–1680 (2008).
6. J. A. Davis, M. J. Mitry, M. A. Bandres, and D. M. Cottrell, "Observation of accelerating parabolic beams," Opt. Express **16**, 12866–12871 (2008).
7. G. A. Siviloglou and D. N. Christodoulides, "Accelerating finite energy Airy beams," Opt. Lett. **32**, 979–981 (2007).
8. G. A. Siviloglou, J. Broky, A. Dogariu, and D. N. Christodoulides, "Observation of accelerating Airy beams," Phys. Rev. Lett. **99**, 213901 (2007).
9. I. M. Besieris and A. M. Shaarawi, "A note on an accelerating finite energy Airy beam," Opt. Lett. **32**, 2447–2449 (2007).
10. G. A. Siviloglou, J. Broky, A. Dogariu, and D. N. Christodoulides, "Ballistic dynamics of Airy beams," Opt. Lett. **33**, 207–209 (2008).
11. I. Dolev, T. Ellenbogen, and A. Arie, "Switching the acceleration direction of Airy beams by a nonlinear optical process," Opt. Lett. **35**, 1581–1583 (2010).
12. Y. Hu, P. Zhang, C. Lou, S. Huang, J. Xu, and Z. Chen, "Optimal control of the ballistic motion of Airy beams," Opt. Lett. **35**, 2260–2262 (2010).
13. J. Broky, G. A. Siviloglou, A. Dogariu, and D. N. Christodoulides, "Self-healing properties of optical Airy beams," Opt. Express **16**, 12880–12891 (2008).
14. M. A. Bandres and J. C. Gutiérrez-Vega, "Airy-Gauss beams and their transformation by paraxial optical systems," Opt. Express **15**, 16719–16728 (2007).
15. H. I. Sztul and R. R. Alfano, "The Poynting vector and angular momentum of Airy beams," Opt. Express **16**, 9411–9416 (2008).
16. L. Carretero, P. Acebal, S. Blaya, C. Garcia, A. Fimia, R. Madrigal, and A. Murciano, "Nonparaxial diffraction analysis of Airy beams and SAiry beams," Opt. Express **17**, 22432–22441 (2009).
17. T. Ellenbogen, N. Voloch-Bloch, A. Ganany-Padowicz, and A. Arie, "Nonlinear generation and manipulation of Airy beams," Nature Photonics **3**, 395–398 (2009).
18. J. Baumgartl, M. Mazilu, and K. Dholakia, "Optically mediated particle clearing using Airy wavepackets," Nature Photonics **2**, 675–678 (2008).
19. A. Salandrino and D. N. Christodoulides, "Airy plasmon: a nondiffracting surface wave," Opt. Lett. **35**, 2082–2084 (2010).

20. A. Chong, W. H. Renninger, D. N. Christodoulides, and F. W. Wise, "Airy-Bessel wave packets as versatile linear light bullets," Nature Photonics **4**, 103–106 (2010).
21. L. Allen, M. W. Beijersbergen, R. J. C. Spreeuw, and J. P. Woerdman, "Orbital angular momentum of light and the transformation of Laguerre-Gaussian laser modes," Phys. Rev. A **45**, 8185–8189 (1992).
22. K. Unnikrishnan, A. R. P. Rau, "Uniqueness of the Airy packet in quantum mechamics," Am. J. Phys. **64**, 1034-1035 (1996).
23. M. Abramowitz and I. A. Stegun, *Handbook of mathematical functions* (Dover, 1965).
24. D. M. Cottrell, A. R. P. Rau, "Direct generation of accelerating Airy beams using a 3/2 phase-only pattern," Opt. Lett. **34**, 2634-2636 (2009).

1. Introduction

In 1979, M. Berry and N. Balazs [1] showed theoretically that the force-free Schrödinger equation has accelerating solutions that are self-similar in time. These solutions are the Airy real functions. Since the force-free Schrödinger equation is equivalent to the equation for the linear propagation of optical beams under the paraxial approximation of diffraction, the Airy functions are also accelerating and non-diffracting solutions of such equation. Actually, although other types of non-diffracting beams have meanwhile been proposed [2, 3, 4], some of them also accelerating as they propagate [5, 6], Airy beams are unique as they are the only type of non-diffracting beams that can exist in a one-dimensional system. An intrinsic characteristic of all these diffraction-free beams is their infinite power, which makes their experimental realization unfeasible. In order to solve this problem, several finite power versions of those non-diffracting beams have been proposed. In particular for Airy beams, attenuated versions of function Ai which are obtained by multiplication of its amplitude by an exponentially decreasing function have been recently proposed [7]. The experimental realization of such finite energy Airy beams (one and two-dimensional) was successfully obtained in 2007 [8]. Even though they are not exact non diffracting solutions, these beams exhibit very interesting properties, such as remaining almost diffraction free as they propagate in the original Ai beam parabolic trajectory for propagation distances that correspond to several diffraction lengths [8, 9], and possibility of controlling their trajectory [10, 11, 12]. Furthermore, these beams show remarkable self-healing properties, tending to reshape after severe perturbations that have been imposed on them, such as blocking parts of the beam and making them propagate in scattering and turbulent media [13]. These peculiar characteristics have attracted a lot of attention from the scientific community [14, 15, 16, 17] and have projected the Airy beams as advantageous optical beams for applications in optical micro-manipulation [18], plasmonic energy routing [19], optical microscopy and scanning microscopy using Airy optical bullets, i.e., linear waves that are both non-diffracting and non-dispersing [20].

Here, we investigate the propagation characteristics of finite energy beams that show some resemblance with Airy beams. In particular, we consider beams with different intensity profiles but with phases always related to the characteristic Airy phase. We start by considering exponentially attenuated Airy beams that have also been blocked on their right edge, and study the effect of the blocking location and attenuation constant on the beam trajectory and profile evolution. Moreover, a new type of non-oscillatory profile derived from Airy functions is also proposed and studied. Finally, we also consider finite width beams with amplitudes either constant or given by the Airy function. The studied beams are also compared regarding initial power requirements for achieving the same propagation distance in the parabolic trajectory and the same peak amplitude.

2. Mathematical formulation

Let us begin by considering the propagation of a plane-polarized optical beam in a linear medium, which is governed by the paraxial equation:

$$i\frac{\partial u}{\partial \xi}+\frac{1}{2}\frac{\partial^2 u}{\partial s^2}=0, \tag{1}$$

where u is the electric field envelope, $s=x/x_0$ and $\xi=z/kx_0^2$ are the dimensionless transverse coordinate and propagation distance, respectively, x_0 is an arbitrary transverse scale, and $k=2\pi n/\lambda_0$ is the wavenumber in a medium with refractive index n.

Looking for solutions of this equation that self-bend while remaining invariant as they propagate, we define an accelerating variable given by $\eta=s-\frac{g}{4}\xi^2+b\xi$ and substitute $u(s,\xi)=W(\eta)\exp[i\theta(\eta,\xi)]$, where both $W(\eta)$ and $\theta(\eta,\xi)$ are real, into Eq. (1), which yields the following ordinary differential equation for $W(\eta)$

$$W''-g\eta W-\frac{A^2}{W^3}=0, \tag{2}$$

and θ given by

$$\theta(\eta,\xi)=A\int_0^{\eta}\frac{d\eta'}{W^2}+\left(\frac{g}{2}\xi-b\right)\eta+\frac{g^2}{24}\xi^3-\frac{gb}{4}\xi^2+\frac{b^2}{2}\xi, \tag{3}$$

where, for simplicity, we assumed that $A=A(\xi)$ was a constant. The complex envelopes $u(s,\xi)$ satisfying Eqs. (2) and (3) are the accelerating nondiffracting solutions of Eq. (1), and are defined as functions of the real constants g and b, which represent, respectively, the acceleration and velocity of the beam's trajectory. Actually, as it was pointed out [10], these beams follow a parabolic trajectory in free-space that is analogous to those of projectiles moving under constant gravity, such that the effect of considering different values of b is equivalent to having different launching angles. Therefore, in the following we will only consider the case $b=0$. Equations (2) and (3) also depend on the real parameter A. In case $A=0$, Eq. (2) becomes equivalent to the well known Airy differential equation. In fact, the change of variable $\zeta=g^{1/3}\eta$ transforms Eq. (2) with $A=0$ into

$$F''-\zeta F=0 \tag{4}$$

where $F(\zeta)\equiv W(\eta)$, which also implies that the degree of freedom introduced by g in the solutions of this dimensionless model is already considered through the arbitrary scale x_0. Hence, the physical situation obtained by changing from g_1 to g_2 would be the same as the one obtained by keeping the same dimensionless acceleration g_1 and choosing another $x_{02}=(g_1/g_2)^{1/3}x_{01}$. For that reason, we consider $g=1$ and $\zeta=\eta$ in the remaining of this text. Under these conditions, the two linearly independent solutions of Eq. (2) are Airy functions $\mathrm{Ai}(\eta)$ and $\mathrm{Bi}(\eta)$. As $\eta\to+\infty$, $\mathrm{Ai}(\eta)$ tends exponentially to zero while $\mathrm{Bi}(\eta)$ grows exponentially. On the other hand, as $\eta\to-\infty$, both $\mathrm{Ai}(\eta)$ and $\mathrm{Bi}(\eta)$ have algebraically decaying oscillations of the same amplitude but differing in phase by $\pi/2$, imposing them infinite energy and making the production of these beams impractical.

As mentioned in the introduction, to overcome the infinite energy physical impediment, exponentially attenuated Airy beams have been recently proposed. At the origin, the field profile of these beams is given by

$$u(s,\xi=0)=\mathrm{Ai}(s)\exp(as) \tag{5}$$

where a is a small positive value that allows containment of the infinite tail while also assuring that the resulting beam still shows a close similarity with function Ai [7]. Even though the

evolution of these finite energy beams is considerably more complex than what is predicted by Eqs. (2) and (3), it is still possible to find a closed form-solution for $u(s,\xi)$ [7], which takes the form

$$u(s,\xi) = \mathrm{Ai}(\eta + ia\xi)\, e^{a\eta - \frac{a}{4}\xi^2}\, e^{i\left(\frac{\eta}{2}+\frac{a^2}{2}+\frac{\xi^2}{24}\right)\xi} \tag{6}$$

where η is defined as before. Besides indicating that the beams will experience peak decay as they propagate, this expression shows that they will diffract as well, as implied by the complex argument of function Ai. Moreover, after some propagation distance, and when the beams have already diffracted considerably, the beams will also abandon their parabolic trajectory. Another interesting property of these beams is their ability to reshape after its main lobe, which contains a relevant part of its total power, has been blocked. In effect, it has been shown that, under certain conditions, blocked beams of this sort are able to reshape in such a way that the reborn part of their profile is more intense than the rest [13], which might indicate that they could exhibit interesting propagation characteristics. Following this result, we decided to simulate the propagation of profiles that result from Airy functions exponentially attenuated to the left, as referred above, as well as blocked to the right of a given zero. Therefore, we shall define

$$\mathrm{Ai}_{nz}(s) = \begin{cases} \mathrm{Ai}(s)\exp(as), & s < a_n \\ 0, & \text{otherwise} \end{cases} \tag{7}$$

as the Ai function that is exponentially attenuated to the left and blocked to the right of its n^{th} zero located at a_n (where $a_1 \simeq -2.3381$, $a_2 \simeq -4.0879$, $a_3 \simeq -5.5206$, ...). For convenience, we will also consider that Ai_{0z} represents the finite-energy beam given by Eq. (5). Similarly, we define

$$\mathrm{Bi}_{nz}(s) = \begin{cases} \mathrm{Bi}(s)\exp(as), & s < b_n \\ 0, & \text{otherwise} \end{cases} \tag{8}$$

as the Bi function that is exponentially attenuated to the left and blocked to the right of its n^{th} zero located at b_n (where $b_1 \simeq -1.1737$, $b_2 \simeq -3.2711$, $b_3 \simeq -4.8307$, ...).

The self-healing process that these beams experience as they propagate can be studied in terms of the transverse component of the average Poynting vector. For paraxial beams it can be shown that [21]

$$\vec{S}_{av} = \frac{1}{2\sqrt{\mu/\varepsilon}}|u|^2\left[\hat{z} + \frac{1}{k}\frac{\partial\alpha}{\partial x}\hat{x}\right] \tag{9}$$

where $\sqrt{\mu/\varepsilon}$ is the intrinsic impedance of the medium and $\alpha(x,z)$ is the phase of u. It is interesting to verify that for the infinite energy Airy beams given by Eqs. (2) and (3) with $A = 0$, we have $\partial\alpha/\partial x = (\xi/2 - b)/x_0$, which for a given ξ is constant and thus explains the diffractionless propagation of these beams. Moreover, it can also be shown that in this case $\vec{S}_{av}$ is tangent in every point to the beams parabolic trajectory [13]. For the finite energy beams, however, the phase evolution is considerably more complex. In effect, not only the magnitude of this energy flux is no longer constant, but also this flux changes sign at different points in the beam, which justifies the beam's diffraction and also its reconstruction.

Equation (2) also exhibits closed-form solutions when $A \neq 0$, which can be written in the form $W(\eta) = \sqrt{\mathrm{Ai}^2(\eta) + A^2\pi^2\mathrm{Bi}^2(\eta)}$. Moreover, since in this case the integral term in Eq. (3) accounts for the phase of $\mathrm{Ai}(\eta) + iA\pi\mathrm{Bi}(\eta)$, as can be easily verified by differentiating both expressions, we conclude that the complex envelope defined by $u(s,\xi=0) = \mathrm{Ai}(s) + iA\pi\mathrm{Bi}(s)$ will also accelerate while remaining invariant. Given that Eq. (1) is linear and that Ai and Bi are solutions of this equation possessing these properties, this result is obviously unsurprising and confirms that Airy beams (Ai or Bi) are the only self-bending non-diffractive solutions of this equation, as was demonstrated in [22].

It can also be pointed out that all the solutions corresponding to $A \neq 0$ have no zeros in their amplitude profiles and, furthermore, their degree of oscillation depends on A. In particular, the solutions with $A = \pm 1/\pi$ also show the very interesting property of exhibiting no oscillations in their amplitude profiles. However, similarly to what happens with Bi, all the solutions corresponding to $A \neq 0$ are divergent for positive s, and thus are impossible to generate or even simulate numerically. For this reason, we will only study here the profile defined by

$$u(s, \xi = 0) = \mathrm{Ai}_{0z}(s) \pm i\mathrm{Bi}_{1z}(s) \tag{10}$$

Note that in this case $|u|$, $\partial|u|/\partial s$ and α are all continuous, whereas $\partial\alpha/\partial s$ is not. It is also relevant to mention that for large $(-s)$ the optical envelope in Eq. (10) approximately satisfies $|u| \propto (-s)^{-1/4}\mathrm{e}^{as}$ and $\alpha \propto \mp\frac{2}{3}(-s)^{3/2}$ [23].

As Eq. (9) suggests, the phase of u plays a predominant role in the trajectory followed by the beam. In effect, it should be noted that, besides Airy beams, the other two-dimensional non-diffracting beams moving along a parabolic trajectory that were recently proposed and observed [5, 6], also exhibit a similar asymptotic behavior of the phase. Moreover, beams showing a close resemblance to Airy beams have also been directly generated by simply imposing a $3/2$ phase-pattern on a constant amplitude [24]. These results served as motivation to further investigate the relation between the parabolic trajectory and the Airy beam phase. For that, several amplitude profiles, other than the blocked profiles defined above, were also used as inputs, all of them having phases similar to the Airy phase.

3. Propagation of exponentially attenuated beams

We have solved Eq. (1) using a FFT based method which monitors the beam evolution on ξ intervals of $\Delta\xi = 0.05$. Thus, the accuracy of any ξ value referred below is limited by this value. Moreover, since our transverse variable was sampled with an interval of $\Delta s = 0.02$, any s value presented below also has this accuracy.

First, we have extensively simulated the propagation of Ai_{nz} and Bi_{1z} for a ranging from 0.01 to 0.3. The propagation of Ai_{0z} and Ai_{3z} when $a = 0.1$ is illustrated in Figs. 1(a)-1(e). Even though both beams are propagating along a parabolic trajectory, their evolution is quite different. Effectively, almost all the energy of beam Ai_{0z} is propagating as a whole, and the peak structure that is characteristic of the initial profile is being lost as it propagates. However, the evolution of Ai_{3z} shows an energy splitting such that the leading part of the profile goes to the right to occupy the place of the missing lobes, which is an evidence of the self-healing mechanism, while the profile trailing part develops a principal lobe followed by a tail, both traveling to the left, thus increasing the separation of both parts. Figures 1(f)-1(h) show the normalized transverse component of Poynting vector, which is obtained from Eq. (9) as $\partial\alpha/\partial s$. There, we may note that the sign of this component is coherent with the evolution of the beams, being negative in the case of movement toward $-s$, and positive otherwise. Furthermore, we found that these two kind of beams stay in the parabolic trajectory for different propagation distances. This can be observed in Fig. 2, which shows the trajectories of the profile maxima for different input profiles corresponding to $a = 0.1$. The initial discontinuities in the trajectory of the blocked beams can be explained by the energy flux that is taking place in these beams, as the blocked part of the beam is being reshaped at the expense of the trailing edge of the pulse, which causes abrupt changes in the location of the profile peak amplitude. It is quite interesting to realize that during this self-healing process, the blocked beams are able to reach exactly the parabolic trajectory of the infinite beam Ai, as if they had the information about the exact position of the initially blocked peak. It was already mentioned that the parabolic trajectory can be explained in terms of an energy flux that depends on the beam's phase derivative. Remember that, for large negative s, Ai and its blocked versions behave like a sinusoidal function of

decreasing period, so we propose that it is the argument of this sinusoid that carries all the necessary information that effectively allows them to reach the parabolic trajectory of the complete Ai function. Moreover, Fig. 2 suggests that the more severe the blocking of these beams is, the longer they stay in this parabolic trajectory.

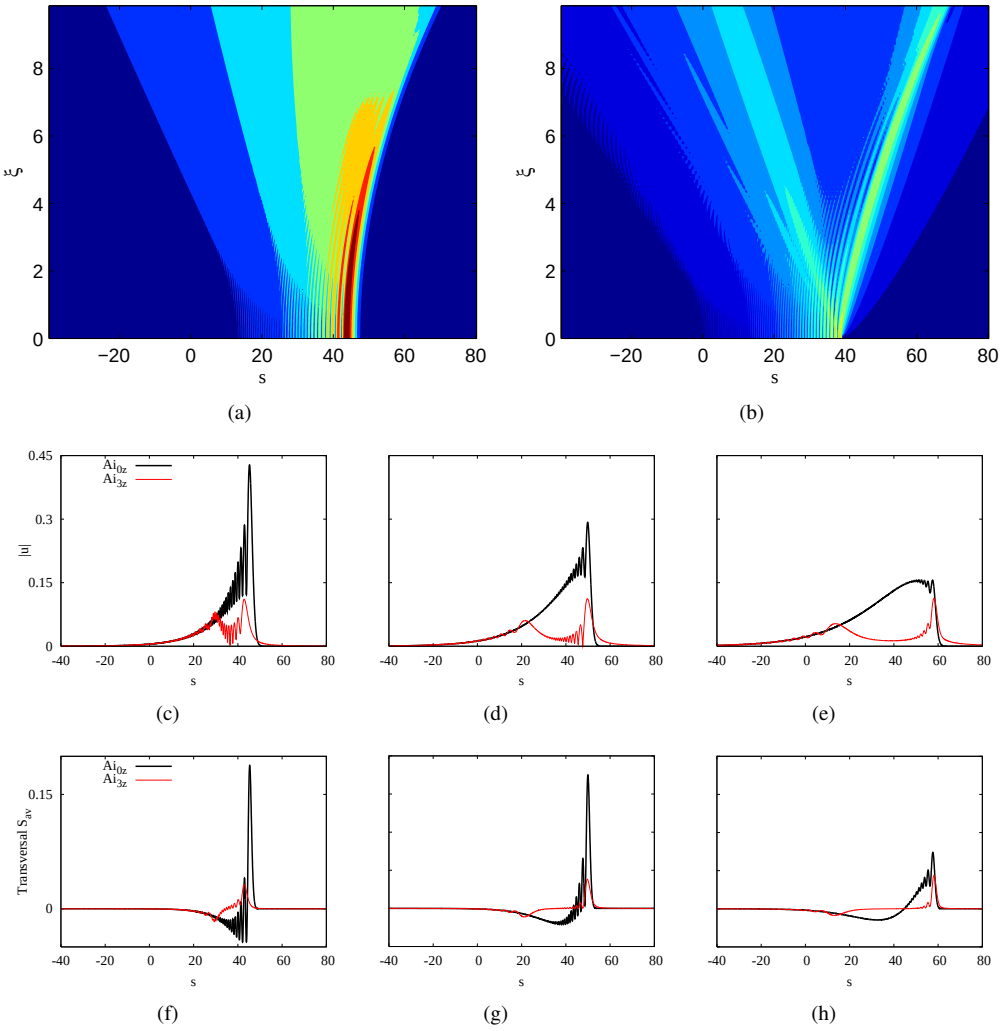

Fig. 1. Propagation dynamics of of (a) Ai_{0z} and (b) Ai_{3z}. Amplitude profiles of both beams at (c) $\xi = 2.5$, (d) $\xi = 5.0$ and (e) $\xi = 7.5$. Normalized transverse component of the average Poynting vector at (f) $\xi = 2.5$, (g) $\xi = 5.0$ and (h) $\xi = 7.5$. Both input profiles have $a = 0.1$.

A further analysis of the trajectory may be done using Fig. 3, where we have plotted the maximum ξ that the beams reach while propagating at the parabolic trajectory, ξ_{final}, as a function of parameter a for different input beams. There, we observe an expected tendency of smaller values of ξ_{final} for larger values of a, since as a increases the larger is the departure of the profile from the infinite Ai solution. We also observe that above a certain a around 0.05, the blocked beams are staying in the parabolic trajectory for longer distances than Ai_{0z}. With these results, we assert that the increase of ξ_{final} as we stronger block Ai only occurs for $a \gtrsim 0.05$.

In order to understand the kind of profile that is arriving at ξ_{final}, we have plotted the intensity

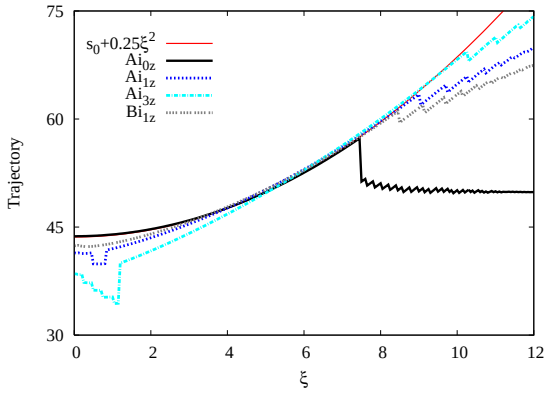

Fig. 2. Trajectories of different inputs, all having $a = 0.1$.

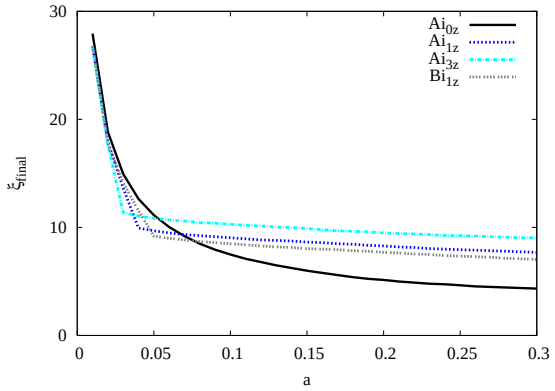

Fig. 3. Maximum ξ reached by the profiles while maintaining their peak at the parabolic trajectory, for different initial inputs.

profiles at ξ_{final} for several Ai_{nz} (see Fig. 4). It was already mentioned that the energy of Ai_{0z} arrives as a whole to ξ_{final}. Furthermore, as Eq. (6) indicates, both the diffraction and the peak attenuation suffered by these beams as they propagate increase with a. Even though this figure suggests exactly the opposite, i. e., that as a increases the output profile is higher in amplitude and thinner in width, it should be noted that ξ_{final} is different for each represented profile and, moreover, that this value decreases with increasing a. On the other hand, the blocked profiles suffer an energy splitting during propagation. The right parts of these beam that have traveled on the parabola have almost the same full width at half maximum for different a but are higher in amplitude for smaller a.

The evolution of the optical envelope given by Eq. (10) also deserves reference. Since Eq. (1) is linear, this evolution can be directly obtained as a superposition of the evolutions corresponding to attenuated beam Ai_{0z} and blocked beam Bi_{1z}. However, it is not straightforward to predict the behavior of the non-oscillatory envelope using the results for beams Ai_{0z} and Bi_{1z}. Actually, it turns out that very different behaviors are obtained when the two signs in Eq. (10) are considered. The beam with the $+$ sign effectively propagates along a parabolic trajectory, whereas the beam with the $-$ sign is evolving to the other side of s. These different trajectories can be easily explained in terms of the transverse Poynting vector given by Eq. (9). When the $+$ sign is

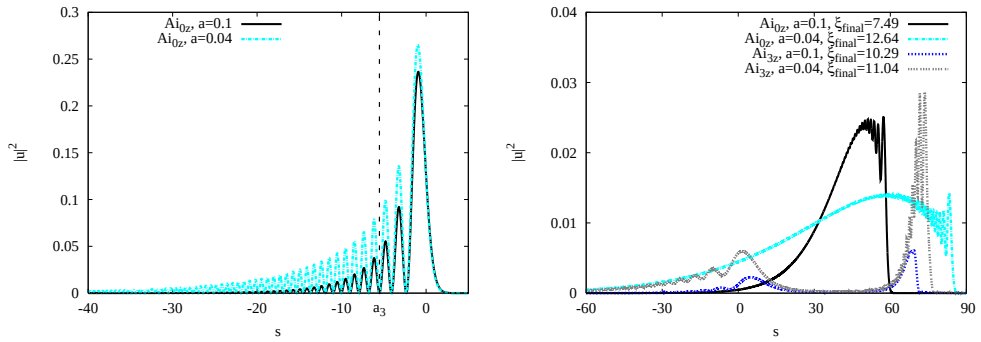

Fig. 4. Intensity profiles at (a) input and at (b) ξ_{final}. The Ai_{3z} versions have the same input profile but are blocked to the right of vertical line.

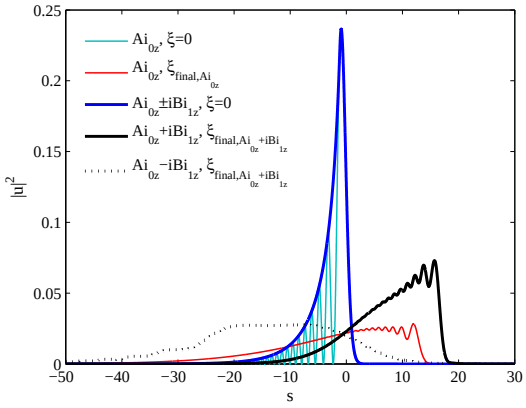

Fig. 5. Intensity profiles at origin and at ξ_{final} for Ai_{0z} and for the non-oscillatory attenuated envelopes with $a = 0.1$. Since Ai_{0z}-iBi_{1z} does not exhibit a parabolic trajectory, its final profile is shown at $\xi_{\text{final,Ai}_{0z}+\text{iBi}_{1z}}$

considered, the phase of the beam increases with s, which means that the transverse component of this vector is positive, and thus the transverse energy flux will be along the $+s$ direction. On the other hand, the phase of the beam associated with the $-$ sign decreases with s, implying transfer of energy towards $-s$, and movement of the beam along this direction. Our simulations have also indicated that the optical envelope given by Eq. (10) with the $+$ sign diffracts less than beam Ai_{0z}, as it is shown in Fig. 5 and also that it says slightly longer in the parabolic trajectory ($\xi_{\text{final,Ai}_{0z}} \simeq 7.25$ while $\xi_{\text{final,Ai}_{0z}+\text{iBi}_{1z}} \simeq 8.25$). Assuming that these beams are propagating in air with $\lambda_0 = 0.5\,\mu$m, and taking x_0 to be $100\,\mu$m, we then have the attenuated Ai_{0z} beam propagating on the parabolic trajectory for approximately 91 cm, whereas the non-oscillatory profile would self-bend for an extra 13 cm. Moreover, the transverse deflections suffered in this case by each beam up to ξ_{final}, which in real units can be calculated from $x_d = \lambda_0^2 z_{\text{final}}^2/(16\pi^2 x_0^3)$, are 1.3 mm and 1.7 mm, respectively for the beams Ai_{0z} and Ai_{0z}+iBi_{1z}. Note that these two deflections actually correspond to approximately 5 and 6.5 times the FWHM of the non-oscillatory profile.

At this point, it should be referred that, even though the energy flux responsible for the bend-

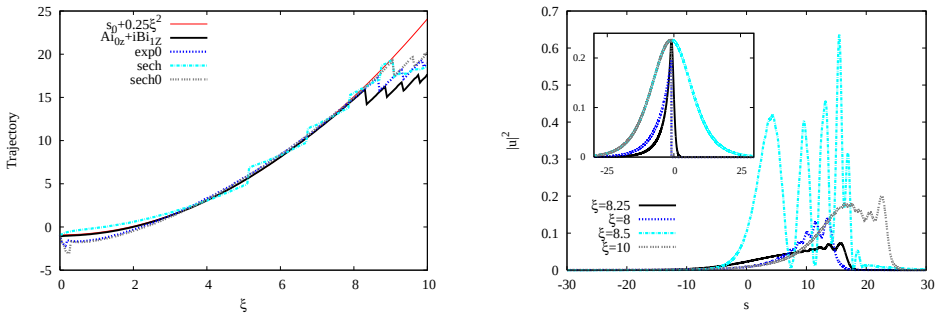

(a) (b)

Fig. 6. (a) Trajectories and (b) intensity profiles at ξ_{final} for several input profiles and respective input profiles in inset.

ing and self-healing of these beams is associated with their phase derivatives, the amplitude profile also plays a very important role. We this in mind, we have simulated the evolution of beams with a phase given by $-\frac{2}{3}(-s)^{3/2}$ for $s < b_1$, and zero otherwise, and with different amplitudes, namely, an exponential amplitude that is blocked to the right of the non-oscillatory beam maximum; an hyperbolic secant profile with a left tail that also evolves as e^{as}; and this hyperbolic secant blocked to the right of its maximum. Our results were compared with the evolution of Ai_{0z}+iBi_{1z} and are illustrated in Fig. 6 for $a = 0.1$. We have found that all the considered beams travel along parabolic trajectories with the same acceleration for some distance. Actually, it turns out that the two hyperbolic secant beams are able to stay in that trajectory for even a longer distance than our non-oscillatory beam. The reason for this might be associated with the higher decay rate of the non-oscillatory beam for small s, which might be interpreted as if the hyperbolic secant effectively had a lower value of a when compared with Ai_{0z}+iBi_{1z}. Moreover, when compared with the other beams, the output profile of the non-blocked hyperbolic secant beam exhibits a large and strongly peaked shape, with a large peak at approximately the initial location of the beam, which can be understood as if the right wing of the initial beam, the part that does not conform with the Ai function, is not self-bending.

Finally, it is also noteworthy pointing out that the exponential amplitude beams provide us a straightforward and convenient means of verifying that it is indeed the phase of the blocked beams that allows them to reach the parabolic trajectory of the infinite Ai. Effectively, since the displacement of an exponential is equivalent to multiplying it by a constant, no relevant information concerning the trajectory can actually be contained in this kind of amplitude, and thus its self-bending could only be explained by the phase profile. We have simulated the propagation of exponential amplitude beams, blocked on the right at different locations s_0, and with the previous approximate phase. The trajectories followed by the beams for $a = 0.04$ and different values of s_0 are summarized in Fig. 7. As expected, even though these beams start their trajectories at different locations, all of them eventually reach the same parabola.

4. Propagation of finite width beams

Our results so far clearly indicate that the distance traveled by the beams on the parabolic trajectory increases as parameter a decreases. This result is obviously unsurprising since the case $a = 0$ corresponds to the infinite Airy beam. As already mentioned, these beams exhibit a very slow decay and, for large negative s, the non-oscillatory profile actually varies as $(-s)^{-1/4}$. This very slow decay might resemble a constant amplitude profile. Since a beam of this sort

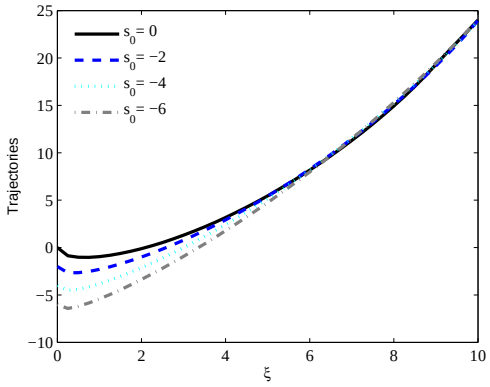

Fig. 7. Trajectory of the amplitude maxima for right blocked exponential amplitude beams with $a = 0.04$ and a phase approximately equal to the phase of Ai_{0z}+iBi_{1z}. The degree of blocking is indicated by s_0.

has an infinite power, a question naturally arises regarding the possibility of having finite width beams with constant amplitude and the previous approximate phase traveling along the same parabolic trajectory. This issue has been recently addressed in [24], where it was experimentally demonstrated that a constant beam with a $3/2$ phase pattern is indeed able to to self-bend according to a parabolic trajectory. Here, we further investigate the evolution of beams of this sort, by simulating the propagation of unitary amplitude beams, extending from $s_e < 0$ to 0, where $|s_e|$ gives the width of these beams, and with a phase given by $-\frac{2}{3}(-s)^{3/2}$ for negative s, and zero otherwise. Figure 8 depicts the trajectories for several values of s_e. Note that, for the ξ considered, the widest beam represented, which has $s_e = -200$, follows a trajectory that coincides with the parabola $s_0 + \xi^2/4$, therefore showing exactly the same acceleration of the complete Ai function. Predictably, as the width of these beams decreases, and thus their left tail diminishes, the trajectories start to depart from this parabola. It is also interesting to verify that, unlike the attenuated beams considered in the previous section, the departure from the parabola is now smooth. The reason for this behavior can be easily understood from the observation of Fig. 9, which illustrates the evolution of the unitary beam extending from -60 to 0. During the initial stage, this beam undergoes considerable compression, which is accompanied by the development of a peaked structure exhibiting a high peak at the leading edge of its profile. The amplitude of this peak grows until the beam stops compressing and diffraction effects take over. For the beam in Fig. 9 this happens at approximately $\xi = 11.5$ and the corresponding peak intensity is around 23.7. Even though the beam diffracts afterwards, and eventually leaves the parabola (at $\xi \simeq 15.5$ for the beam with $s_e = -60$), its maximum stays at the leading edge of the profile. This is in contrast with the attenuated Airy beams studied, for which the departure of the parabolic trajectory coincided with the change in the location of the peak. Furthermore, the shape of the intensity profile at ξ_{final} is also quite different for these constant amplitude beams and the attenuated Ai beams. Effectively, by comparing the profile at ξ around 15.5 in Fig. 9 with the output intensity profiles of the Ai_{0z} and Ai_{0z}+iBi_{1z} beams represented in Fig. 5, we clearly see that the first shows a much larger and narrower peak than the other two. It turns evident that this high peak might represent an advantage in some practical applications. Moreover, the generation of this kind of beams could be simpler than the attenuated Ai beams, since now little more than a phase mask is required, using a method identical to what has been proposed in [24]. It is also noteworthy to point out that Airy-related finite width beams have already been proposed [16]. These beams were designated as SAiry beams and are generated

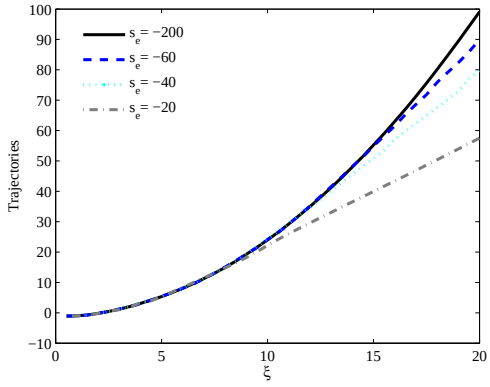

Fig. 8. Trajectories of finite width constant amplitude beams, extending from s_e to 0, with phase similar to Ai_{0z}+iBi_{1z}.

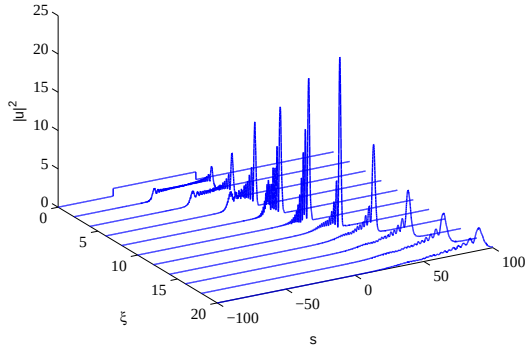

Fig. 9. Evolution of a unitary amplitude beam of width 60 and with phase similar to Ai_{0z}+iBi_{1z}.

at the focal plane of a lens that is illuminated by a constant amplitude beam with a cubic phase. Even though they are not the same as the finite-width beams here studied, it is nevertheless interesting to verify that in the case of SAiry beams a high intensity peak was also obtained.

A natural issue raised by these constant amplitude beams is their input power, specially when compared with the attenuated Ai beams. However, when that comparison is made by choosing beams with the same ξ_{final} which have also their input amplitudes adequately adjusted so that they have equal peak intensities at ξ_{final}, we find that the power of constant amplitude beams is actually much lower than the one of attenuated Airy beams. As an example, let us consider again the constant amplitude beam with $s_e = -60$, which has $\xi_{\text{final}} \simeq 15.5$. The attenuated Ai_{0z} beam with the same ξ_{final} corresponds to $a = 0.028$ and its input power is $\int |u|^2 ds = 1.19$. Moreover, the peak amplitude of this beam at ξ_{final} is only 0.1065, whereas the corresponding value for the constant amplitude beam with unitary input amplitude is 2.72. Therefore, by adjusting the constant beam initial amplitude to give the same peak amplitude at ξ_{final}, we determine its input power to be 0.092, that is, only 7.7% of the attenuated Ai beam power. Analogous results were obtained in other cases.

The very interesting propagation characteristics of the previous finite width beams motivated us to also investigate the propagation of the finite energy Airy beams that are originated by

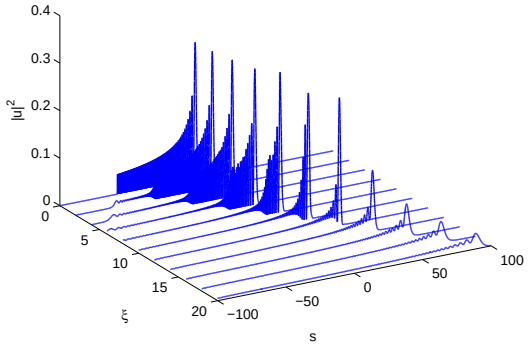

Fig. 10. Evolution of the finite width Ai beam with $s_e = -58$.

simply blocking the infinite Ai beam to the left of a given s_e. Our simulation results indicate that, as these beams propagate, they undergo an evolution showing some similarities to the one described above. In particular, the output profile also exhibits a high peak, although not as pronounced as before, and this high peak is located at the leading edge of the intensity profile. For illustration purposes, let us consider the finite width Ai beam corresponding to $s_e = -58$ (see Fig. 10), which leaves the parabolic trajectory at $\xi_{\text{final}} = 15.4$ with a peak amplitude of 0.288, and has a input power of 2.4243. When the amplitude of this beam is adjusted in such a way that its output peak amplitude is equal to the one of the Ai_{0z} beam with $a = 0.028$, which has approximately the same value of ξ_{final}, we find that the input power of the finite width Ai beam is only 27.9% of the Ai_{0z} power. This again represents a power saving, yet not as dramatic as the one already mentioned. In effect, when comparing the two referred finite width beams for the same output peak amplitude, we obtain that the input power of the constant amplitude beam is only 27.6% of the finite Ai_{0z} beam. This seems to suggest that constant amplitude beams are advantageous when looking for a given output peak amplitude.

5. Conclusions

We studied blocked versions of exponentially attenuated Airy beams and found that for strongly attenuated beams the parabolic trajectory is better followed by the blocked beam versions than by the attenuated only version. Moreover, we found a close interdependence between the parabolic trajectory of the Airy beams and their characteristic phase, such that, other kind of amplitude profiles having the same phase travel in the same parabola. Some of these modified Airy beams show enhanced propagation characteristics, namely, output profiles showing less diffraction effects, as in the case of the non-oscillatory profile, and a very good ratio of output peak amplitude to input power, as in the case of constant amplitude finite width beams.

Acknowledgments

This publication was supported by FCT within the scope of *Financiamento do Laboratório Associado INESCPorto* and *Financiamento do Laboratório Associado I3N-Aveiro*. We thank the reviewers for valuable suggestions that contributed to improve this paper.